2024 IEEE/RSJ International Conference on Intelligent Robots and Systems (IROS)
October 14-18, 2024. Abu Dhabi, UAE

Low-Cost Air Hockey Robot Using a Five-Bar Linkage Mechanism Driven by Position-Control Servomotors

Mirai Shinjo[1], Cristian C. Beltran-Hernandez[1], Masashi Hamaya[1], and Kazutoshi Tanaka[1]

***Abstract*— In human-robot interaction (HRI) research, ball games pose significant challenges that demand robotic solutions that are both cost-effective and user-friendly for non-experts. Air hockey, characterized by safe, non-direct-contact play and a simplified state-action space, emerges as an ideal platform for such research. Despite the availability of various air hockey robots, their high cost and complexity have limited widespread use among researchers requiring robotics expertise. Addressing this gap, we introduce a low-cost, accessible air hockey robot designed to facilitate HRI studies. Featuring a lightweight five-bar linkage mechanism powered by low-cost servomotors for position control, this robot combines efficiency with ease of use. The complete robot's cost is estimated at $346.8, with the arm weighing a mere 19 grams. The robot precisely returns the puck by intermittently adjusting its target joint positions, achieving a play with an average return error of 42.6 mm. These characteristics affirm the robot's potential as a valuable tool for advancing HRI research.**

I. INTRODUCTION

Ball games contain non-verbal, physical, and cognitive interactions and provide many robotic challenges in human-robot interaction (HRI) research, such as entertaining humans [1], motivating humans [2], and improving human ability [3]. A robotic research platform is indispensable to tackle these HRI challenges. Researchers have developed several ball game robots, such as table tennis [4], badminton [5], and volleyball [6]. Air hockey suits the HRI challenges because of the following advantages.

- Safer than other ball games as the players are never in direct contact
- Simpler state and action space: just two players' mallets hitting the puck in the two-dimensional playing field

The simpler space makes the ball game interaction analysis and design easier. Researchers have developed many air hockey robots, such as ones estimating a fast-moving puck's state [7], [8], ones planning their high-speed motion [9], ones learning control [10], and ones with a game strategy [11]. However, these robots typically used an expensive arm and high-end sensors, needed large spaces to set up, and required robotic expertise to operate. Therefore, this work aims to develop a low-cost air hockey robot research platform that researchers without robotic expertise can operate.

Using low-cost, low-power motors for air hockey robots is challenging because the robots should accelerate their arm quickly and move them fast to respond to and hit a fast-moving puck. Therefore, high-cost, commercially available, general-purpose arms, such as WAM Arm (Barret Technology) [8] and LWR (KUKA) [10], have been used for air hockey robots. Decreasing the weight of the moving links using specific actuation mechanisms, such as linkage ones [12] and cable-driven ones [13], enables our robotic arm to increase motion speeds using lower-cost, lower-power motors. Especially, locating all motors of the robotic arm at the base link using linkage mechanisms [14] and cable-driven mechanisms [15] decreases the weight of the moving links. A simple five-bar linkage mechanism can have motors at the base link and move an articulated 2-degrees-of-freedom (DoF) arm in a horizontal plane. Therefore, we adopted the five-bar linkage mechanism to design our air hockey.

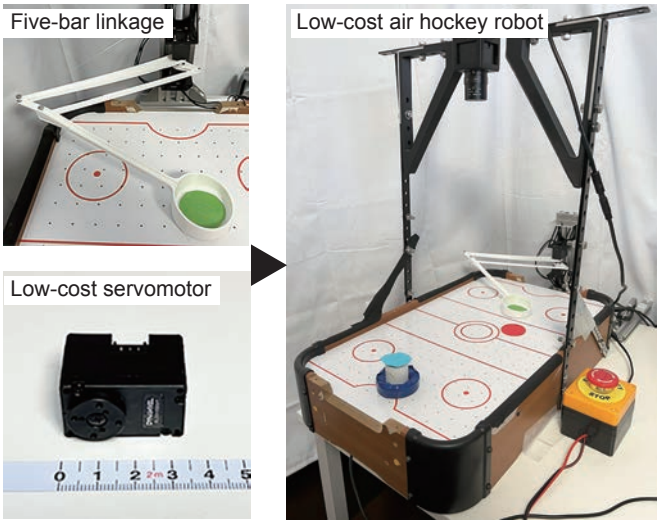

Fig. 1. Low-cost air hockey robot. This robot has a five-bar linkage mechanism for fast motions. The robot generates a hitting motion to return the puck to the target location using position-control servomotors by setting the target joint position intermittently.

Position-control servomotors suit an air hockey robot for the HRI research as some products of these servomotors are commercially available, have lower costs than other motors, and can decrease the cost of robots. The servomotors are equipped with a motor driver in their body, which simplifies the electric system of robots. Researchers without robotic expertise can use them by sending target joint angles. Therefore, they have been used for robots, such as a cable-driven arm [16], dual-arm [17], and robot hand [18], which researchers without robotics expertise can use. We also adopted them for our air hockey robot.

*This work was supported by JST, PRESTO Grant Number JPMJPR22C6, Japan.

[1]M. Shinjo, C. Cristian, M. Hamaya, and K. Tanaka are with OMRON SINIC X Corporation, Hongo 5-24-5, Bunkyo-ku, Tokyo, Japan kazutoshi.tanaka@sinicx.com

To return the puck to the target location, other air hockey robots planned their end effector's continuous target trajectory. These robots moved the end effector to follow the trajectory by controlling their joint velocity sequentially at high frequency (e.g., 500 Hz [8]). In contrast, using the position control servomotors, our robot requires setting its joint positions intermittently, i.e., at low frequency (10 Hz). Therefore, we propose an alternative hitting motion generation method for our robot to generate a hitting motion to return the puck to the target location. Using this method, the robot moves the end effector through the via location on a line with the target location and hitting location.

We developed a hockey robot that is low-cost and easy to use for researchers without robotic expertise using a five-bar linkage mechanism and position-control servomotors, as shown in Fig. 1. The main contributions of this study are summarized below.

- Low-cost air hockey robot that is open hardware and software[1] to the benefit of the HRI research community
- Novel design of a horizontal arm using a five-bar linkage mechanism to decrease the weight of the moving links and to increase motion speed
- Hitting motion generation method where the end effector goes through the via location on a line with the target location and hitting location

The remainder of this paper is organized as follows: Sec. II summarizes the related works. Sec. III introduces the robot's hardware with the five-bar linkage mechanism. Sec. IV describes the robot's software using the hitting motion generation method. Sec. V presents the experimental results. Finally, Sec. VI concludes the paper.

II. Related work

A. Air hockey robots

Many air hockey robots have been developed over the past two decades. Bishop and Spong developed an air hockey robot with a 3 DoF horizontal articulated arm using vision-based control [19]. Liu et al. presented a high-speed air hockey robot using a 7 DoF lightweight arm that planned its motion effectively and reactively Bayesian optimization [9]. Namiki et al. developed an air-hockey robot with a 4 DoF cable-driven arm using high-speed vision sensors [8]. Tadokoro et al. presented an air hockey robot using a WAM arm with a high-speed wrist [20]. Tab. I summarizes the features of these robots, comparing them with our robot. We estimate the robots' lower cost limits based on the prices of their arms. The table indicates that an air hockey field and our arm are smaller, and our cost is lower than the robots. Whereas the air hockey robots had a large arm, used large air hockey fields, and needed large spaces, our air hockey robot has a small arm, plays air hockey in a small field, and can be used in a compact space, as shown in Fig. 2.

High-cost arms have been used for air hockey robots to follow the planned continuous path of their end effector by sequentially controlling the velocity of these arms to return the puck to the target location accurately. Namiki et al. generated a hitting motion of their air hockey robot by calculating the inverse kinematics, deciding the joint angles at the hitting timing, generating the joint trajectory, and controlling the joints to follow the trajectory [8]. Fukuda et al. presented an air hockey robot that planned the trajectory of its end effector and followed it using nonlinear model predictive control to hit the puck [11], [21]. In contrast to these robots, our air hockey robot generates a hitting motion by intermittently setting the target joint positions.

[1]https://github.com/omron-sinicx/air-hockey-robot-v1

TABLE I
Air hockey robots

	Cost [$]	Field size (LxW) [m]	Arm DoF	Frame rate [fps]
Ours	**347**	**0.48x0.28**	2	30
[19]	—	1.75x0.88	3	30
[8]	> 135000	2.07x1.01	4	**500**
[20]	> 135000	2.07x1.01	5	**500**
[9]	> 7000	2.16x1.22	**7**	120

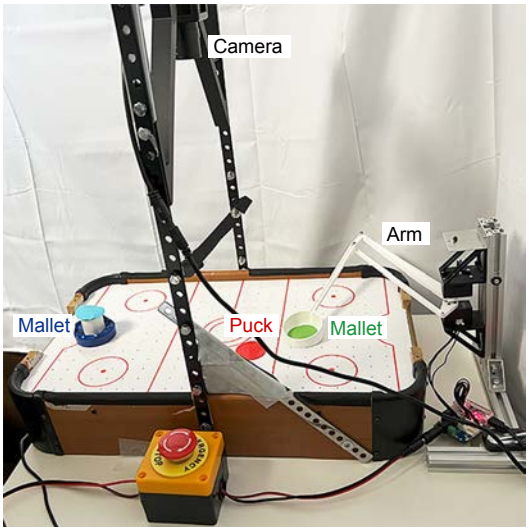

Fig. 2. Appearance of our air hockey robot. The robot plays air hockey on a table with a human in a compact space.

B. Five-bar linkage mechanisms

Linkage mechanisms have been used to decrease the weight of moving links and increase the speed of robots. Han et al. proposed a humanoid leg design with a four-bar linkage mechanism in the knee and ankle to place all the actuators at the hip [22]. Gim et al. presented a humanoid leg design that combined serial and parallel linkage mechanisms [23]. Asai et al. developed a high-speed table tennis robot using a parallel robot with linkage mechanisms [12].

A five-bar linkage mechanism is one of the simplest linkage mechanisms. Using a five-bar linkage mechanism, Asada and Youcef-Toumi presented a direct-drive arm [24], Campos et al. developed an arm with a large workspace [25], Kenneally et al. introduced direct-drive-legged robots [26], and Tanaka et al. proposed a quadruped free-climbing robot [27]. Whereas the robotic limbs in these robots had rigid links to

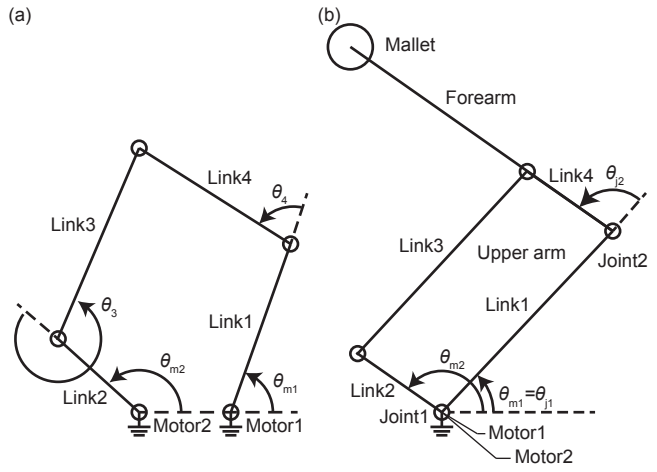

Fig. 3. Mechanics of (a) a general five-bar linkage mechanism and (b) a five-bar mechanism in our robot.

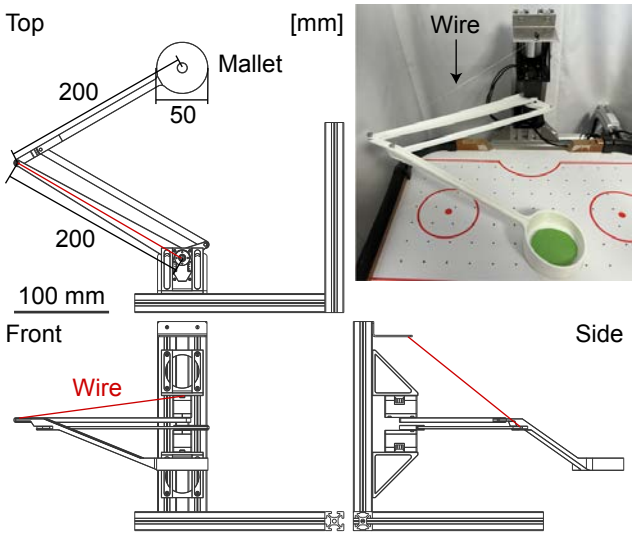

Fig. 4. Dimensions and appearance of the arm.

carry heavy payloads, our arm has lightweight, thin links to move its lightweight end effector.

III. Arm with a Five-Bar Linkage Mechanism

Our robot has a five-bar linkage mechanism to remove motors from moving links, decrease the weight of these links, and increase the motion speed.

A. Five-bar linkage mechanism

Fig. 3 shows the mechanics of the general five-bar linkage mechanism and that of our air hockey robot arm. Motor1 and motor2 are fixed to the base link, motor1 rotates link1, motor2 drives link2, and link3 and link4 move along the pose of link1 and link2. One joint connects the end of link3 to the end of link4. Therefore, the angles in the mechanism have the following relationships.

$$L_1\cos\theta_{\mathrm{m1}} + L_4\cos(\theta_{\mathrm{m1}}+\theta_4) = X_2 + L_1\cos\theta_{\mathrm{m2}} + L_4\cos(\theta_{\mathrm{m2}}+\theta_3) \quad (1)$$

$$L_1\sin\theta_{\mathrm{m1}} + L_4\sin(\theta_{\mathrm{m1}}+\theta_4) = Y_2 + L_1\sin\theta_{\mathrm{m2}} + L_4\sin(\theta_{\mathrm{m2}}+\theta_3), \quad (2)$$

where L_i is the length of link$\{i\}$, θ_{m1} and θ_{m2} are the angles of motor1 and motor2, θ_3 is the angle between link2 and link3, θ_4 is the angle between link1 and link4, and (X_2, Y_2) is the relative location of the axis of motor2 from that of motor1. Motor1 and motor2 control link1 and link2, respectively, and the end positions of link1 and link2 determine the pose of link3 and link4. The pose of link4 in the general five-bar linkage mechanism shown in Fig. 3(a) is controlled by calculating its kinematics based on Eq. (1) and Eq. (2) [28].

As illustrated in Fig. 3(b), our robot's arm had a five-bar linkage mechanism with a specific structure to mitigate the complexity of the link angle relationships in a general five-bar linkage. In the arm, motor1 and motor2 share the same rotation axis, and the pair of link1 and link3 and the pair of link2 and a proximal part of link4 have the same length, respectively. Then, the angles of motor1 and motor2 determine the angles between the links in a simple manner:

$$\theta_{\mathrm{j1}} = \theta_{\mathrm{m1}} \quad (3)$$

$$\theta_{\mathrm{j2}} = \theta_{\mathrm{m2}} - \theta_{\mathrm{m1}}, \quad (4)$$

where θ_{j1} and θ_{j2} are the angles of joint1 between link1 and link4 and joint2 between link2 and the base link, respectively. The robot calculates the target motor angles $\tilde{\theta}_{\mathrm{m1}}$ and $\tilde{\theta}_{\mathrm{m2}}$ from $\tilde{\theta}_{\mathrm{j1}}$ and $\tilde{\theta}_{\mathrm{j2}}$ using Eq. (3) and Eq. (4). The robot determines the target joint angles, $\tilde{\theta}_{\mathrm{j1}}$ and $\tilde{\theta}_{\mathrm{j2}}$, from the target mallet position $\tilde{x}_{\mathrm{R}} = (X_{\mathrm{R}}, Y_{\mathrm{R}})$ based on the equations

$$X_{\mathrm{R}} = L_1\cos\theta_{\mathrm{j1}} + L_{\mathrm{f}}\cos(\theta_{\mathrm{j1}}+\theta_{\mathrm{j2}}) \quad (5)$$

$$Y_{\mathrm{R}} = L_1\sin\theta_{\mathrm{j1}} + L_{\mathrm{f}}\sin(\theta_{\mathrm{j1}}+\theta_{\mathrm{j2}}), \quad (6)$$

where L_{f} is the forearm's length.

B. Arm with the mechanism

Fig. 4 shows the drawing and appearance of the arm. The arm has 2 DOF to move the mallet in the planar field. The lengths of both the forearm and upper arm are 200 mm so that the robot can reach the mallet at all locations in its half of the field. The mallet is combined with the forearm, the links are made of 3D-print nylon parts, and the nylon wire connects the end of the forearm and the top of the base frame to avoid bending the forearm link by gravity.

The arm is actuated by low-power, low-cost two position-control servomotors (Dynamixel XL330-M288-T, ROBOTIS). An electric power of 6 V is supplied to the motors.

The weights of the forearm and upper arm are 19 g and 11 g, respectively. The weight of the motor is 18 g. Using a five-bar mechanism and removing the motors from the moving links decreases the $18/(19+11+18)\times 100 = 37.5$ % weight of the arm at least.

TABLE II
SPECIFICATION

Total size	300x600x500 (WxLxH) mm
Total weight	1.4 kg
Arm length	400 mm
Arm moving links weight	30 g
Motor	Dynamixel XL330-M288-T, ROBOTIS
Camera	USBFHD01M-SFV, ELP

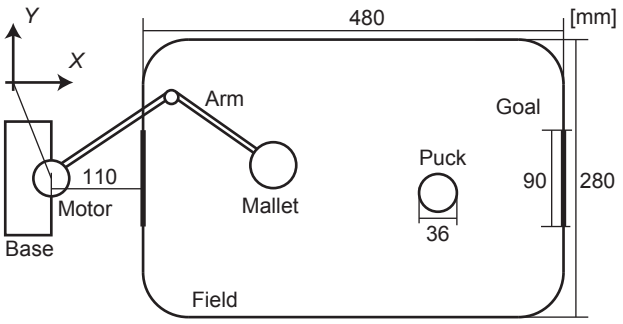

Fig. 5. Dimension of our air hockey robot and the world coordinate.

C. Air hockey robot with the arm

Tab. II lists the robot's specifications. Fig. 5 shows the dimensions and world coordinates. We selected a tabletop-size air hockey field for our robot to decrease the size and cost of both the robot and the field, decrease the space required for experiments, and make it easier for our robot to use, as described above. The size of the air hockey field is 480x280 mm (LxW). The goal width of the field is 90 mm, and the diameter and thickness of the puck are 36 mm and 2 mm, respectively. The robot motor axis matches the origin of the world coordinates. The sidewalls of the air hockey field are parallel to the X axis.

The robot has a camera (USBFHD01M-SFV, ELP) on top of the field to observe the positions of the puck, the robot's mallet, and the human player's mallet. The camera captures images of the air hockey field at 30 fps. It was calibrated using a checkerboard to correct lens distortion.

Tab. III presents the cost breakdown of the robot. The total cost is \$346.80. The cost of the motors includes a communication module and an electric supply module. The cost is calculated assuming that $\$1 = ¥140$. Using low-cost servomotors (Dynamixel XL330-M288-T, \$23.90) reduces the total cost. Employing other lower-cost compatible power supplies and using a different camera could further decrease the total cost.

IV. HITTING MOTION GENERATION

Our air hockey robot leverages position-control servomotors, unlike other air hockey robots, as described above. Therefore, our robot generates a hitting motion using a method where the end effector goes through the via location on a line with the target location and hitting location by intermittently setting the target joint positions. We introduce our robot's software and this method in the section.

TABLE III
COST BREAKDOWN OF THE ROBOT

Motors	\$98.90
Camera	\$48.00
Power supply	\$99.30
Mechanical parts	\$51.60
Air hockey field	\$20.70
Total	\$346.80

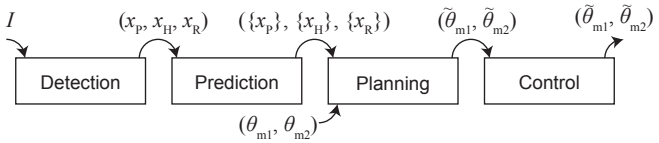

Fig. 6. Software modules of our air hockey robot arm. I: a visual image. x_{P}: is a puck location, x_{H}: is a human mallet location, and x_{R}: is a robot mallet location. θ_{m1}: a motor1 angle. θ_{m2}: a motor2 angle. $\{x\}$ is predicted future locations. $\tilde{\theta}$: the target motor angle.

A. Software of the robot

When playing air hockey, a robot recognizes the air hockey puck, anticipates the puck's future locations, plans a hitting motion, and controls the arm to execute this motion. Thus, the software of our air hockey robot contains a detection module, prediction module, planning module, and control module, as shown in Fig. 6.

The detection module obtains a visual image I from the camera, recognizes the puck and the human mallet in I, and detects the location of the puck x_{P} and human mallet x_{H}. The prediction module calculates the velocity of the puck and anticipates its future locations $\{x_{\mathrm{P}}\}$. We describe the details of the detection module in Appendix A and the prediction module in Appendix B.

The planning module determines the target location of the robot mallet $\tilde{x}_{\mathrm{R}}$, and hitting timing $\tilde{t}$. This module calculates the target motor angles θ_{m} from $\tilde{x}_{\mathrm{R}}$, as described in Sec. III-A. Our robot plans a hitting motion to return the puck to the target location. We introduce the details of planning this hitting motion in the next section.

The robot also executes a block motion to save its goal. For this block motion, a block line in front of the goal on the robot's side is set in advance. In the block motion, the robot moves its mallet to a location on this block line to block the puck. When planning the motion, the robot selects the target robot's mallet location $\tilde{x}_{\mathrm{R}}$ from the pack's future locations $\{x_{\mathrm{P}}\}$ such that $d < r_{\mathrm{P}}$, where d is the distance between $\tilde{x}_{\mathrm{R}}$ and the block line and r_{P} is the radius of the puck.

The control module receives $\tilde{\theta}_{\mathrm{m}}$ and sends $\tilde{\theta}_{\mathrm{m}}$ to the servomotors. Note that other air hockey robots, using velocity control, planned a continuous path of the robot mallet in their planning module and sequentially controlled their joint velocity to follow this path in their control module. In contrast, our air hockey robot, using position control, determines the target motor angles in its planning module and sends these angles to its control module.

To run the software modules, we used the robot operating

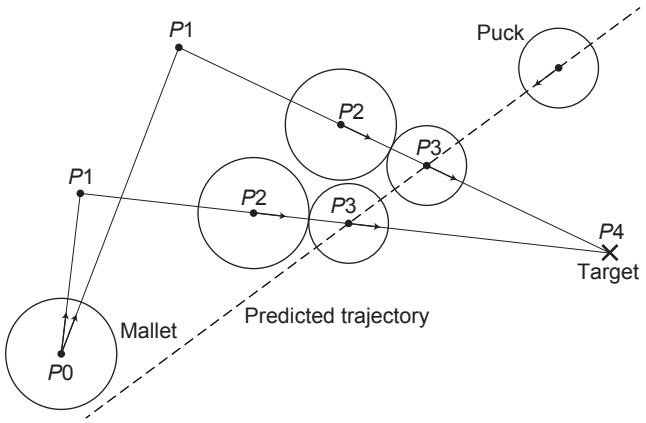

Fig. 7. Planning of hitting the puck. The dotted line represents the anticipated pack's future locations.

system (ROS2) [29] to easily test hypotheses by simply changing one module. For example, researchers can test a robotic strategy to increase user satisfaction by changing only the planning module.

B. Hitting motion planning

First, we explain the aim of our hitting motion planning. Other air hockey robots planned their end effector's continuous trajectory and have moved the end effector to follow it by sequentially controlling joint velocity, as described above. In contrast, using position-control servomotors, our robot plans its hitting motion by intermittently setting the target joint angles. Therefore, the robot decides a sequence of the target motor joint angles such that the position and velocity of the robot's end effector satisfy the condition where the effector collides with the puck and the condition where the puck reaches the target location after hitting.

Second, we introduce our assumptions. As the weight of the robot mallet is significantly larger than that of the puck, we made the following assumptions.

- The robot mallet velocity immediately before hitting determines the puck velocity immediately after hitting.
- The puck reaches the target location after hitting if the robot mallet moves on a line with the target location and the puck location immediately before hitting.

Third, we describe the target robot mallet location sequence based on our assumptions. Our robot plans the sequence to hit the puck, as shown in Fig. 7. In this figure, $P0$ is the initial robot mallet location, $P1$ is a via location, $P2$ is the robot mallet location when hitting, $P3(\in \{x_{\mathrm{P}}\})$ is the puck location when hitting, and $P4$ is the target puck return location. Our robot moved its mallet to $P2$ from $P0$ via $P1$ to hit the puck at $P3$. Points $P1$, $P2$, $P3$, and $P4$ are collinear. Thus, $P1$ is calculated from $P3$ and $P4$ using

$$\frac{P1 - P4}{d_{13} + d_{34}} = \frac{P3 - P4}{d_{34}}, \tag{7}$$

where $d_{ij} = |P\{j\} - P\{i\}|$. We set $d_{13} = 70$ mm in advance. Note that our arm can return the puck to the target location but cannot guarantee its end effector to accurately follow a line between $P0$ and $P1$ or another line between $P1$ and $P2$ using position-control servomotors that can only control motor joint angles.

Finally, we present the determination of the target robot mallet locations, $P1$ and $P2$. Using Eq. (7), $P1$ and d_{01} are calculated from each $P3$ in $\{x_{\mathrm{P}}\}$. To reach $P1$ in the shortest time, $P3$ that minimizes d_{01} is selected, which satisfies $P1 \in A$ and $P2 \in A$, where A is the robot's reachable area. The target robot mallet locations, $P1$ and $P2$, are obtained from the selected $P3$ using Eq. (7).

V. Experiment

In the experiments, we verified the performance of our robot's block and hitting motions to clarify whether the robot has a basic capacity to play air hockey. Appendices C, D, and E show the experimental results of mallet motion speed, repeatability, and mallet position accuracy, respectively, as other basic robot performance metrics.

A. Block success ratio

We evaluated the block success ratio. A human hit the puck, the robot executed block motions, and we counted the number of successful blocks and calculated the block success ratio. We set (X, Y) =(250, 0), (280, 0), and (330, 0) mm as the initial robot mallet location in each trial and $X =$ 210 mm and $-100 < Y < 100$ mm as the block line. The coordinates are shown in Fig. 5. It was more difficult for the robot to save its goal in the (X, Y) =(330, 0) condition where the initial location was farther from its goal than that in other conditions.

The human hit 100 times, and the robot successfully blocked the puck 91, 90, and 85 times in conditions with the (250, 0), (280, 0), and (330, 0) initial positions, respectively. These results indicate that the robot can perform block motions.

B. Hit-back location accuracy

We evaluated the location accuracy of the puck that the robot hit and returned. We set (590, -71) mm as the right target position and (590, 71) mm as the left target position in front of the human goal side. We sent the puck around the center of the field from the center on the human side. The robot hit the puck to the right target 20 times and the left target 37 times. To evaluate the hit-back location accuracy, we measured the distance of the target position from the line on which the puck moved after hitting.

Our robot returned the puck to the target location as shown in Fig. 8. The distance for the condition with the right target point was 42.6 ± 41.7 mm, and that for the condition with the left target point was 74.6 ± 48.56 mm (mean $\pm$ standard deviation), respectively. These results suggest that the robot can return the puck to the target location.

VI. Conclusions

This study presented a low-cost air hockey robot using a five-bar linkage mechanism and position-control servomotors. Researchers without robotics expertise can easily use

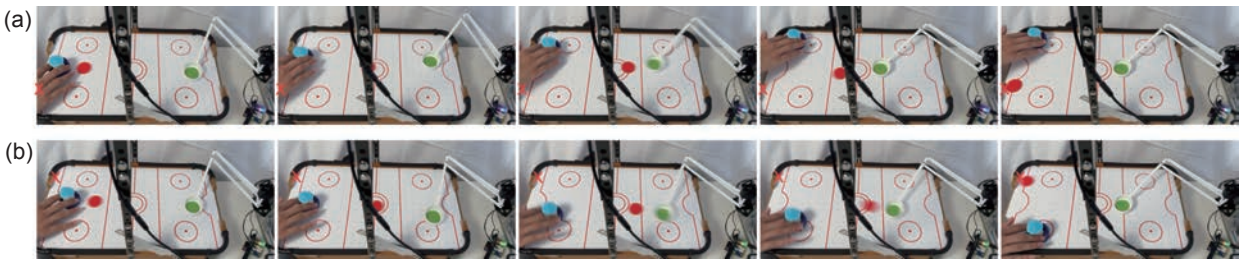

Fig. 8. Snapshots of the hitting motion. The red x indicates the target location to which the puck is returned. (a) Left target and (b) right target.

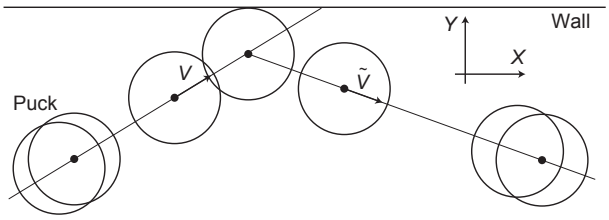

Fig. 9. Reflexion model of the puck against a wall.

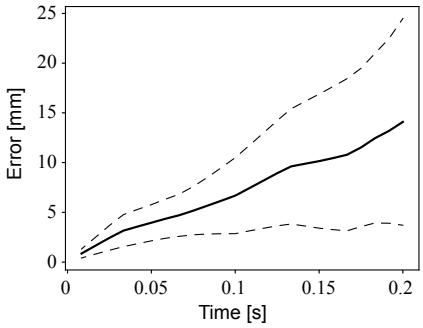

Fig. 10. Puck prediction errors without reflection. The solid and dotted lines represent the mean and standard deviation of prediction errors, respectively. $n = 16$.

this robot to address the HRI challenges. Our proposed robot costs $346.80. In experiments, the robot defends a puck with a 91% success rate and hits a puck with an average 42.6 mm error from the target location. These results demonstrate the basic capacity to play air hockey. Future work will involve HRI research using this air hockey robot, such as planning a game strategy for entertaining the human player.

APPENDIX

A. Puck detection

Due to its low computational cost, we applied the HSV to detect the puck. The detection module can calculate the puck's location using HSV even if the puck moves fast and a blur occurs. The module calculates the HSV of this visual image, binarizes the image based on HSV values using predefined thresholds to detect the pixels of the puck, processes morphology operations to remove noise, and calculates the center of mass of the image as the puck position. It converts the puck's location in the image into one in world coordinates. A round, blue paper is attached to the top of the human player's mallet. The module also detects the location of the mallet using HSV.

B. Puck prediction

Assuming that the puck and the human player's mallet move at a constant speed, the prediction module anticipates their future locations based on their current position and velocity. Fig. 9 illustrates the reflection model of a puck against a wall. Assuming that the reflection of the puck against a wall and the mallet is an inelastic collision and that the side walls of the field are parallel to the X axis of the world coordinates, as described above, the puck velocity immediately after reflecting against a side wall, $v = (\tilde{v}_X, \tilde{v}_Y)$ is calculated from the velocity immediately before hitting, $v = (v_X, v_Y)$ as $\tilde{v}_X = v_X, \tilde{v}_Y = -kv_Y$, where v_ζ is the ζ composion of the v and k is an elastic coefficient. We set $k = 0.7$.

C. Puck prediction accuracy

We measured the puck's location and collected the puck's predicted locations to evaluate the prediction module's accuracy. A human played air hockey with a robot that executed block motions with a block line for one minute to collect data in preliminary experiments. This data was collected at a time when after hitting by the human and before the reflection against the walls and hitting by the robot. Then, we calculated the errors between the measured and predicted locations of the puck.

Fig. 10 illustrates the prediction errors. This figure shows that the errors increased as the prediction length increased. The mean of the errors of 0.2 s future locations is 14.1 mm, which is smaller than the 18 mm radius of the puck.

D. Robot mallet speed

To evaluate the robot mallet's motion speed, we measured the time required to move the mallet to distant target points from the initial center point. We set $(X, Y) = (250, 0)$ mm as the initial point and $(X, Y) = (330, -80)$ mm, $(330, 80)$ mm, $(170, 80)$ mm, and $(170, -80)$ mm as the target points. The robot moved the mallet 50 times toward each target point.

Fig. 11 (a) shows the robot mallet trajectories. This figure shows that one mallet trajectory to one target point and other

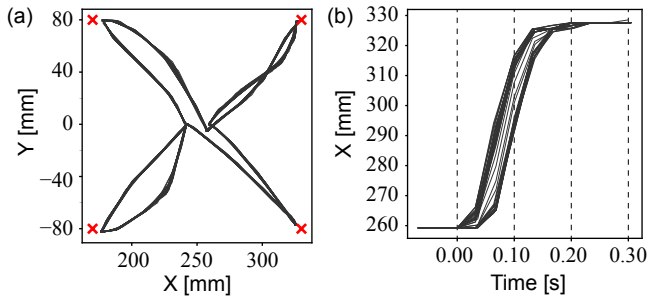

Fig. 11. (a) Robot mallet trajectories. (b) Robot mallet position sequences to the target point $(330, 80)$. The motor commands were sent at $t = 0$ s.

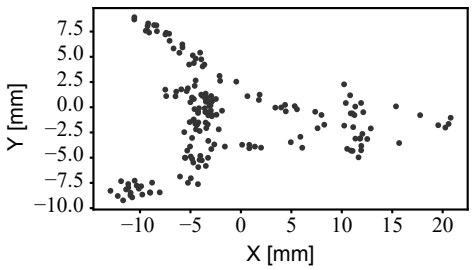

Fig. 12. (a) Position difference of the robot mallet from the target point.

trajectories to this target point go through nearby locations. These trajectories are curved because the motors move at a constant speed.

Fig. 11 (b) illustrates robot mallet position sequences for the target point $(X, Y) = (330, 80)$ mm. This figure shows that the mallet started the motion at 0.05 s after the motor commands were sent and reached the target point in 0.25 s. The time to move to the target points is 0.17 ± 0.02 s (mean $\pm$ standard deviation). To evaluate the repeatability, we calculated the differences of the robot mallet position from the average at each time point in the sequences, the standard deviation of the X and Y components of the differences, and the average of the standard deviation. The average of the X and Y standard deviations are 3.5 mm and 4.3 mm, respectively.

E. Motion accuracy

To evaluate the accuracy of the robot mallet motion endpoint, we randomly changed the target point in an area, $170 < X < 330$ mm, $-80 < Y < 80$ mm, that was farther from the initial point than 60 mm, moved the robot mallet at the maximum speed from the initial point of (250, 0) mm to the target point, and measured the position difference between the robot mallet and the target point.

Fig. 12(a) illustrates these differences. The X and Y components of the absolute error values from the target point are 6.72 ± 4.10 mm, 3.49 ± 2.80 mm, and 7.97 ± 4.30 mm (mean $\pm$ standard deviation), respectively. The maximum error of the X component, Y component, and the size of the difference were 20.79 mm, 9.23 mm, and 20.82 mm, respectively.

ACKNOWLEDGMENT

We would like to thank Y. Fuchioka for the useful discussions.

REFERENCES

[1] J. Kober, M. Glisson, and M. Mistry, "Playing catch and juggling with a humanoid robot," in *IEEE-RAS International Conference on Humanoid Robots*. IEEE, 2012, pp. 875–881.

[2] A. Sackl, D. Pretolesi, S. Burger, M. Ganglbauer, and M. Tscheligi, "Social robots as coaches: How human-robot interaction positively impacts motivation in sports training sessions," in *IEEE International Conference on Robot and Human Interactive Communication*. IEEE, 2022, pp. 141–148.

[3] K. Sato, K. Watanabe, S. Mizuno, M. Manabe, H. Yano, and H. Iwata, "Development and assessment of a block machine for volleyball attack training," *Advanced robotics*, vol. 31, no. 21, pp. 1144–1156, 2017.

[4] K. Mülling, J. Kober, O. Kroemer, and J. Peters, "Learning to select and generalize striking movements in robot table tennis," *The International Journal of Robotics Research*, vol. 32, no. 3, pp. 263–279, 2013.

[5] S. Mori, K. Tanaka, S. Nishikawa, R. Niiyama, and Y. Kuniyoshi, "High-speed and lightweight humanoid robot arm for a skillful badminton robot," *IEEE Robotics and Automation Letters*, vol. 3, no. 3, pp. 1727–1734, 2018.

[6] H. Nakai, Y. Taniguchi, M. Uenohara, T. Yoshimi, H. Ogawa, F. Ozaki, J. Oaki, H. Sato, Y. Asari, K. Maeda *et al.*, "A volleyball playing robot," in *IEEE International Conference on Robotics and Automation*, vol. 2. IEEE, 1998, pp. 1083–1089.

[7] S. Rezvankhah, A. A. Bagherzadeh, H. Moradi, and B. N. Araabi, "A real-time velocity estimation using motion blur in air hockey," in *IEEE International Conference on Robotics and Biomimetics*, 2012, pp. 1767–1772.

[8] A. Namiki, S. Matsushita, T. Ozeki, and K. Nonami, "Hierarchical processing architecture for an air-hockey robot system," in *IEEE International Conference on Robotics and Automation*, 2013, pp. 1187–1192.

[9] P. Liu, D. Tateo, H. Bou-Ammar, and J. Peters, "Efficient and reactive planning for high speed robot air hockey," in *IEEE/RSJ International Conference on Intelligent Robots and Systems*, 2021, pp. 586–593.

[10] A. Xie, D. Losey, R. Tolsma, C. Finn, and D. Sadigh, "Learning latent representations to influence multi-agent interaction," in *Conference on robot learning*. PMLR, 2021, pp. 575–588.

[11] S. Fukuda, K. Tadokoro, and A. Namiki, "Motion strategy using opponent player's serial learning for air-hockey robots," in *IEEE/RSJ International Conference on Intelligent Robots and Systems*, 2021, pp. 952–957.

[12] A. Kyohei, N. Masamune, and Y. Satoshi, "The ping pong robot to return a ball precisely," *OMRON TECHNICS*, vol. 51, pp. 1–6, 2020.

[13] Y.-J. Kim, "Anthropomorphic low-inertia high-stiffness manipulator for high-speed safe interaction," *IEEE Transactions on robotics*, vol. 33, no. 6, pp. 1358–1374, 2017.

[14] V. Nabat, M. de la O Rodriguez, O. Company, S. Krut, and F. Pierrot, "Par4: very high speed parallel robot for pick-and-place," in *IEEE/RSJ International Conference on intelligent robots and systems*. IEEE, 2005, pp. 553–558.

[15] K. Tanaka and M. Hamaya, "Twist Snake: Plastic table-top cable-driven robotic arm with all motors located at the base link," in *IEEE International Conference on Robotics and Automation*, 2023, pp. 7345–7351.

[16] M. Quigley, A. Asbeck, and A. Ng, "A low-cost compliant 7-dof robotic manipulator," in *IEEE International Conference on Robotics and Automation*, 2011, pp. 6051–6058.

[17] T. Z. Zhao, V. Kumar, S. Levine, and C. Finn, "Learning fine-grained bimanual manipulation with low-cost hardware," in *Robotics: Science and Systems*, 2022.

[18] R. Ma and A. Dollar, "Yale openhand project: Optimizing open-source hand designs for ease of fabrication and adoption," *IEEE Robotics & Automation Magazine*, vol. 24, no. 1, pp. 32–40, 2017.

[19] B. Bishop and M. Spong, "Vision-based control of an air hockey playing robot," *IEEE Control Systems Magazine*, vol. 19, no. 3, pp. 23–32, 1999.

[20] K. Tadokoro, S. Fukuda, and A. Namiki, "Development of air hockey robot with high-speed vision and high-speed wrist," *Journal of Robotics and Mechatronics*, vol. 34, no. 5, pp. 956–964, 2022.

[21] A. Namiki and T. Ozeki, "Vision-based optimal control for an air-hockey robot system," in *IEEE International Conference on CYBER Technology in Automation, Control, and Intelligent Systems*. IEEE, 2017, pp. 1176–1181.
[22] S. Han, S. Um, and S. Kim, "Mechanical design of robot lower body based on four-bar linkage structure for energy efficient bipedal walking," in *IEEE International Symposium on Safety, Security, and Rescue Robotics*, 2016, pp. 402–407.
[23] K. G. Gim, J. Kim, and K. Yamane, "Design of a serial-parallel hybrid leg for a humanoid robot," in *IEEE International Conference on Robotics and Automation*, 2018, pp. 6076–6081.
[24] H. Asada and K. Youcef-Toumi, "Analysis and design of a direct-drive arm with a five-bar-link parallel drive mechanism," *Journal of Dynamic Systems, Measurement, and Control*, vol. 106, no. 3, pp. 225–230, 09 1984.
[25] L. Campos, F. Bourbonnais, I. A. Bonev, and P. Bigras, "Development of a five-bar parallel robot with large workspace," in *International Design Engineering Technical Conferences and Computers and Information in Engineering Conference*, vol. 44106, 2010, pp. 917–922.
[26] G. Kenneally, A. De, and D. E. Koditschek, "Design principles for a family of direct-drive legged robots," *IEEE Robotics and Automation Letters*, vol. 1, no. 2, pp. 900–907, 2016.
[27] Y. Tanaka, Y. Shirai, X. Lin, A. Schperberg, H. Kato, A. Swerdlow, N. Kumagai, and D. Hong, "Scaler: A tough versatile quadruped free-climber robot," in *IEEE/RSJ International Conference on Intelligent Robots and Systems*. IEEE, 2022, pp. 5632–5639.
[28] M. E. Kütük and L. C. Dülger, "A hybrid press system: Motion design and inverse kinematics issues," *Engineering Science and Technology, an International Journal*, vol. 19, no. 2, pp. 846–856, 2016.
[29] S. Macenski, T. Foote, B. Gerkey, C. Lalancette, and W. Woodall, "Robot operating system 2: Design, architecture, and uses in the wild," *Science Robotics*, vol. 7, no. 66, p. eabm6074, 2022.